Medicine Meets Virtual Reality 11, J.D. Westwood et al. (Eds.), IOS Press, January 2003, pp. 19-25.

Simulating Needle Insertion and Radioactive Seed Implantation for Prostate Brachytherapy

Ron Alterovitz[*], Jean Pouliot[†], Richard Taschereau[†], I-Chow Joe Hsu[†], and Ken Goldberg[*]
[*]*IEOR & EECS Departments, UC Berkeley*
[†]*Department of Radiation Oncology, UC San Francisco*

Abstract. We are developing a simulation of needle insertion and radioactive seed implantation to facilitate surgeon training and planning for brachytherapy for treating prostate cancer. Inserting a needle into soft tissues causes the tissues to displace and deform: ignoring these effects during seed implantation leads to imprecise seed placements. Surgeons should learn to compensate for these effects so seeds are implanted close to their pre-planned locations. We describe a new 2-D dynamic FEM model based on a 7-phase insertion sequence where the mesh is updated to maintain element boundaries along the needle shaft. The locations of seed implants are predicted as the tissue deforms. The simulation, which achieves 24 frames per second using a 1250 triangular element mesh on a 750Mhz Pentium III PC, is available for surgeon testing by contacting ron@ieor.berkeley.edu.

1. Introduction

During brachytherapy, a type of minimally invasive surgery, surgeons insert radioactive seeds into cancerous tumors. This approach has rapidly gained popularity for treating prostate cancer due to the excellent long-term outcomes. The success of this procedure depends on the accurate placement of radioactive isotopes within a known volume of prostate cancer. Using ultrasound guidance, a real-time image of the implant volume can be seen and the position of each implant needle can be adjusted to ensure proper placement. Once in place, the seeds (each the size of a grain of rice) irradiate surrounding tissue. The dose delivered should minimize healthy tissue damage while maximizing the destruction of cancerous cells.

A dosimetric plan is prepared before the implant procedure. Positions of the seeds are determined to provide a good dose distribution including a minimum peripheral dose coverage, a uniform dose distribution, and the protection of the urethra. Methods for calculating optimal seed locations are available [1, 2]. The relative coordinates of the seeds are then used by the surgeon for seed implantation within the prostate. Approximately 100 seeds and biodegradable spacers are loaded into 20 to 25 needles. The surgeon inserts each needle transperineally into the patient, who is lying on his back. Seeds and spacers are ejected from the needle when the depth of the needle specified by the plan is reached. Achieving this desired seed placement is left to the surgeon, who must take into account tissue deformations during the implant process [3-5]. Unfortunately, inserting and retracting a needle in soft tissues causes the tissues to move, stretch and deform. This displacement and distortion of the prostate during the implantation results in misplaced seeds [4, 6], as demonstrated in Figure 1. The surgeons must therefore learn to compensate for these effects in an attempt to drop the seeds accurately in the prostate to the planned

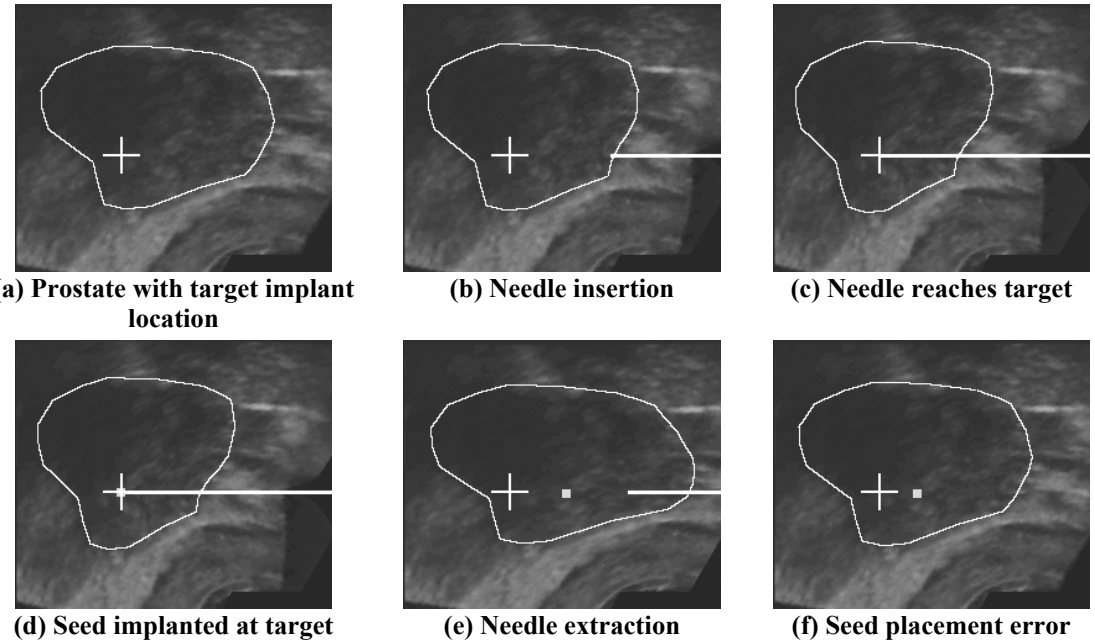

(a) Prostate with target implant location **(b) Needle insertion** **(c) Needle reaches target**

(d) Seed implanted at target **(e) Needle extraction** **(f) Seed placement error**

Figure 1: Simulation of needle insertion based on an ultrasound image of a human prostate cancer patient. Frame (a) outlines the prostate and the target implant location (white cross) which is fixed in the world frame. Our simulation places a radioactive seed (small square) at this location (d). After needle retraction, the placement error, the distance between the target and resulting seed location shown in (f), is 20% of the width of the prostate. Needle plans that compensate for tissue deformation can reduce placement errors like these that damage healthy tissue and fail to kill cancerous cells.

positions.

To help surgeons train for this type of surgery, we are developing a dynamic simulation of needle insertion and radioactive seed implantation during prostate brachytherapy. Our fast FEM based algorithm calculates the deformation and displacement of soft tissues and predicts seed positions during needle insertion and retraction. Unlike other methods such as the mass-spring model, the finite element method (FEM) is based on the equations of continuum mechanics. Real-time visual performance for surgery simulation of the human liver using FEM was achieved by Cotin et al. using a large preprocessing step [7]. They modeled tissue as a linearly elastic material and allowed only small quasi-static deformations. The quasi-static assumption was relaxed by [8-10], who simulated dynamic deformations of soft materials. Real-time performance was accomplished using mass lumping, an approach we also use.

DiMaio and Salcudean performed pioneering work in simulating the deformations that occur during needle insertion [11]. They used a quasi-static finite element method that achieves extremely fast update rates (500Hz) and high accuracy, but requires a calibration phase where the force distribution along the needle shaft is estimated based on observed tissue deformations. Unfortunately, this force distribution, which is modeled with a parameterized surface, may be difficult to measure in vivo. We propose an alternative model based on a reduced set of scalar parameters such as needle friction, sharpness, and velocity.

2. Organ Model

A 2-D slice of the prostate and the surrounding tissue is defined using a mesh of triangular elements. This *reference mesh* G defines the shape of the tissues where the i'th node is located at the point (x_i, y_i). This mesh can be deformed by applied forces (caused by needle insertion) to displace each node by $(u_{x,i}, u_{y,i})$, where $u_{x,i}$ is the displacement of the x degree

of freedom (DOF) of node i. The *deformed mesh* G' is constructed so that each node i is located at $(x_i+u_{x,i}, y_i+u_{y,i})$. For visualization, mesh G is used to obtain texture-map image coordinates for G' (Figure 2).

We approximate the prostate and surrounding soft tissues as linearly elastic homogeneous materials. Our parameterized model requires values for tissue density, stiffness, and compressibility, as well as the force required to cut a unit length of tissue, the force required to break the prostate membrane, and the static and kinetic coefficients of friction for the needle. These parameters were estimated so that the simulation closely reproduced an ultrasound video of needle insertion in a patient, as explained in section 5.

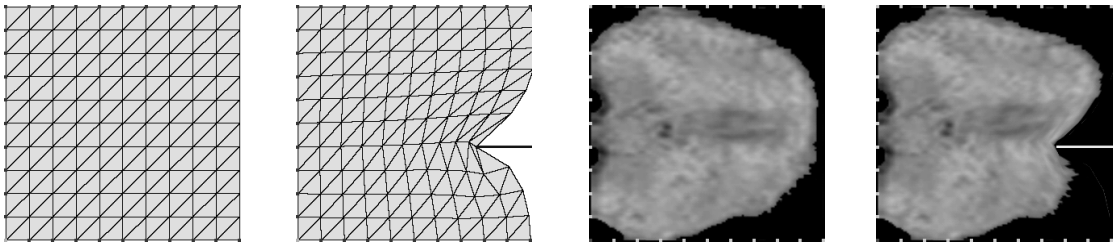

Figure 2: An applied force causes a deformation to reference mesh G to produce deformed mesh G'. Mesh G is used to obtain texture coordinates for G'.

3. Computing Soft Tissue Deformations

We use the finite element method (FEM) to compute the deformations of soft tissues when forces are applied. Rather than calculating only static deformations, we simulate the dynamic behavior of soft tissues. Hence, we must solve for the acceleration, velocity, and position of each node for every simulation frame that is displayed. The time-step duration is adaptive; it is set using the system clock to the amount of time that has passed since the last simulation frame was displayed.

The soft tissue is defined by a mesh composed of *m* discrete triangular elements created using *n* nodes, each with 2 degrees of freedom. The FEM problem is defined by a system of 2*n* linear differential equations [12]:

$$\mathbf{M}\,\mathbf{a}_i + \mathbf{C}\,\mathbf{v}_i + \mathbf{K}\,\mathbf{u}_i = \mathbf{f}_i \qquad \text{[Equation 1]}$$

where **M** is the mass matrix, **C** is the damping matrix, **K** is the stiffness matrix, $\mathbf{f}_i$ is the external force vector, $\mathbf{a}_i$ is the nodal acceleration vector, $\mathbf{v}_i$ is the nodal velocity vector, and $\mathbf{u}_i$ is the nodal displacement vector at time-step i.

The vector $\mathbf{f}_i$ represents the forces exerted by the needle on the tissue, as described in section 4. The matrices **M**, **C**, and **K** are properties of the material being modeled and are constructed by superimposing the element mass, damping, and stiffness matrices [12]. These matrices must be updated if a node is constrained or moved.

To solve for the unknown vectors $\mathbf{a}_i$, $\mathbf{v}_i$, and $\mathbf{u}_i$ for the current time-step i, we use the Newmark method [13], which can be used to translate [Equation 1] into an explicit linear system. Mass lumping, which approximates the continuous material as a particle system, decouples this system of equations into a set of algebraic equations, each of which can be solved in constant time without any pre-computation [8-10]. Mass lumping results in a small loss of accuracy in the dynamics of the object, as shown experimentally [14]. The resulting explicit system of equations produces stable simulations for interactive time-steps because the time-step length is inversely proportional to the natural frequency of the dynamic system in [Equation 1], which is very small for soft tissues [8].

4. Simulating Surgical Needle Insertion

During brachytherapy for treating prostate cancer, a needle carrying radioactive seeds is guided through soft tissues to the prostate. We break down the procedure for each needle into 7 phases:

1. Tissue compression: The needle is inserted through soft tissue and pushes against the prostate membrane.
2. Membrane puncture: The needle punctures the prostate membrane.
3. Insertion: The needle moves deeper into the prostate.
4. Tissue settling: When the needle stops moving, the tissue settles to a stable state.
5. Implantation: A radioactive seed is implanted in the tissue at the needle tip.
6. Retraction: The needle is removed.
7. Equilibrium: The tissue, containing the implanted seed, returns to a stable state.

Phases 3 through 6 can be repeated, particularly for needles carrying multiple seeds.

The forces applied during needle insertion and retraction are described in [15]. These include:

1. Cutting force at the needle tip
2. Friction between the needle shaft and tissue
3. Stiffness of the tissue

The different phases of brachytherapy are modeled by setting appropriate values for the forces listed above. Before entering the prostate, the needle cuts through the surrounding fatty tissue, which requires a low cutting force at the needle tip. The prostate membrane requires a higher cutting force to penetrate, causing tissue compression. Frictional forces are applied throughout needle insertion and retraction. The FEM solver handles tissue settling and equilibrium automatically since it calculates deformations at every time-step.

As in brachytherapy, the surgeon must select an insertion height for the needle. We assume the needle moves left parallel to the horizontal x-axis. For the simulation, we also assume that the needle is thin, rigid, and symmetric along its axis.

4.1 Simulating Cutting at the Needle Tip

Let point **p** be the location of the needle tip. At all times during needle insertion, a node c is constrained to be located at the needle tip point **p** and a list of nodes constrained along the needle shaft is stored in memory. Let ***i***, ***j***, and ***k*** be the nodes of a triangular element, as shown in Figure 3. The needle tip at node c=***i*** is moving horizontally to the left as shown by the vector **r**' in Figure 3.b. This vector is linearly transformed to the reference mesh in Figure 3.a and is denoted by **r**. We assume that the x-component of **r** is always negative. In the reference mesh, vector **r** intersects the segment formed by nodes ***j*** and ***k*** at the point **q**. Let f_c be the force applied by the needle at node c and let f_b represent the magnitude of the force required to cut a length b of tissue. When $f_c \geq f_b$, the tip of the needle moves a distance b along **r** in the reference mesh to a new point $\mathbf{p}+b\mathbf{r}$.

As **p** approaches **q** in Figure 3, it is necessary to prevent a collision of node ***i*** with the

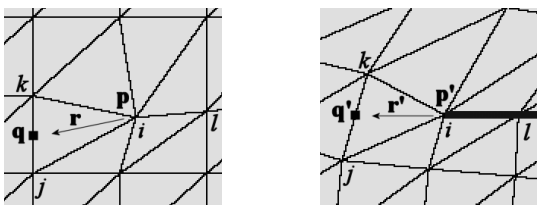

(a) Reference Mesh **(b) Deformed Mesh**

Figure 3: The reference and deformed meshes. The needle's tip is at node c=***i*** at point **p**.

segment (***j***,***k***). Node ***l*** is the first node on the needle shaft behind the tip node. When the distance from node ***l*** to node ***i*** is more than twice the distance from node ***i*** to point **q**, node ***i*** is added to the needle shaft: the x-component of node ***i*** is freed and the node is constrained to lie on the needle axis by fixing its y-component DOF. The closer of node ***j*** or ***k*** is moved to **p**+*b***r** and is defined as the new tip node *c*. Key frames from a simulation using this type of mesh modification are shown in Figure 4. When the elements are sufficiently small, this method produces a stable simulation.

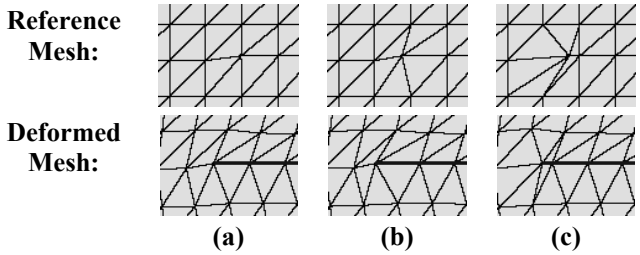

Figure 4: The needle tip moves to the left in (a) through (c). The tip node is moved onto the shaft in (c) and the next tip node is selected.

4.2 Simulating Membrane Puncture

The membrane surrounding the prostate is defined as a polygon whose vertices are points defined in the reference mesh. The location of the membrane vertices in the deformed mesh can be found using the shape functions of the enclosing elements and the displacement of the element nodes [12] in constant time. The force required to puncture the prostate membrane is greater than the force required to cut through soft tissue. Hence, when the needle tip is about to cross an edge of the membrane, a membrane cutting force f_m is used instead of the standard soft tissue cutting force f_b.

4.3 Simulating Friction Along the Needle

Our approach to modeling static and kinetic friction between the needle shaft and the tissue is based on [16]. When the tangential velocity of a node along the needle shaft and the velocity of the needle are equal to within a small threshold v_s, then static friction is applied: the node is attached to the needle and moves at the same velocity. When the tangential force f_s required to attach the node to the needle exceeds the slip force parameter $f_{s\text{-}max}$, then the x-component of the node is freed so the node can slide along the needle shaft. When the tangential velocity exceeds a threshold parameter v_k, a dissipative force f_k is applied to the node. The threshold v_k must be greater than v_s to prevent oscillations after large time-steps. The dissipative frictional force should be proportional to the normal force of the tissue against the needle. We assume a constant normal force, which is reasonable during single needle insertion when the needle is of constant thickness.

4.4 Simulating Radioactive Seed Implantation

A seed is implanted at point **s** by moving the needle tip location **p** to point **s** in the reference mesh. We assume that the seed does not move in the reference mesh after it is implanted. The location of **s** in the deformed mesh is found using the same method as for vertices of a membrane as described in section 4.2.

5. Simulation Performance

The simulator was implemented in C++ using OpenGL on a 750Mhz Pentium III PC with 128MB RAM. Using a mouse, a user can select the height of the needle and guide the needle to the desired target (Figure 6). For a model with 1250 triangular elements the simulator responds at the rate of 24 frames per second, sufficient for visual feedback (but not fast enough for haptic control).

To evaluate model accuracy, we compare ultrasound images taken from a real surgical procedure with images generated by the simulator. In June 2002, a needle insertion procedure was performed in the operating room at the UCSF Medical Center and recorded with an ultrasound probe. A sequence of ultrasound image frames, in which needle position is visible, was recorded. Using only the first frame to locate the prostate and membrane, the simulation generates a mesh deformation that simulates the organ's response to the needle. A texture map of the first frame of ultrasound is then deformed based on this mesh to produce the simulation. This simulation is compared with true ultrasound frames in Figure 5. Although it is difficult for non-specialists to identify organ boundaries in ultrasound, UCSF surgical experts comparing the two image sequences judged them as remarkably similar.

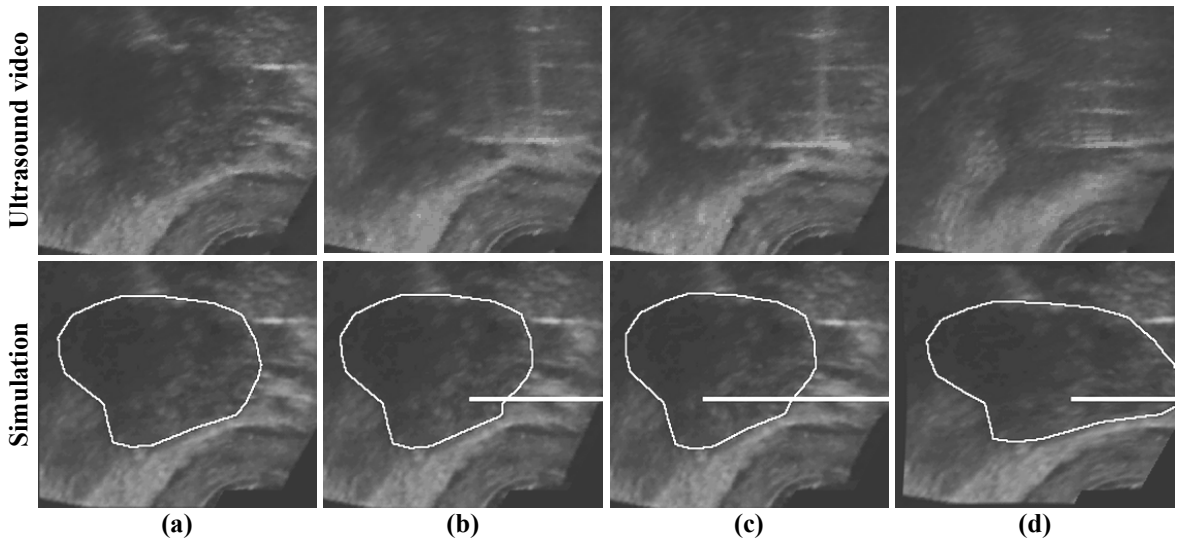

Figure 5: A comparison of frames from the ultrasound video to snapshots from the simulation. The initial ultrasound video frame is used as the texture-map for the simulation snapshots. A polygon defining the prostate is shown in the simulation. The simulator predicts with reasonable accuracy the tissue deformations that occur in the operating room during needle insertion.

6. Conclusions

This paper describes a new 2-D simulation based on a dynamic FEM formulation and a 7-phase insertion sequence where the FEM mesh is updated to maintain element boundaries along the needle shaft. The computational complexity of the model grows linearly with the number of elements in the mesh and achieves interactive performance on standard PC's. The simulation provides an environment for surgeon training and in the future will be applied to dosimetry planning.

We are very interested in feedback from practicing surgeons. The simulator can be downloaded and run on any Windows PC using the mouse to direct needle insertion. Please contact us at ron@ieor.berkeley.edu.

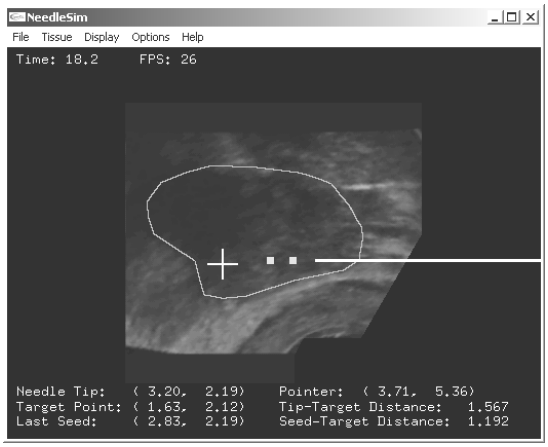

Figure 6: The simulation user interface, which is based on an ultrasound image, is intended to mimic the experience of a surgeon performing brachytherapy. The surgeon interactively guides the needle using a mouse and implants seeds (small squares). Tissue deformations and seed locations are predicted and displayed. The implantation error is the distance between the seed and its target (cross) at equilibrium.

7. Acknowledgements

We thank Russ Taylor, Tim Salcudean, Simon DiMaio, K. Gopalakrishnan, Dezhen Song, M. Cenk Cavusoglu, Frank van der Stappen, and Han-Wen Nienhuys for their feedback and advice.

8. References

[1] J. Pouliot, D. Tremblay, J. Roy, and S. Filice. Optimization of Permanent 125I Prostate Implants using Fast Simulated Annealing. Int.J.Radiat. Onco. Biol. Phys. 1996; 36(3): 711-720.

[2] E. Lee, R. J. Gallagher, and M. Zaider. Planning Implants of Radionuclides for the Treatment of Prostate Cancer: An Application of Mixed Integer Programming. Optima March 1999; 61.

[3] J. E. Dawson, T. Wu, T. Roy, J. Y. Gy, and H. Kim. Dose effects of seeds placement deviations from pre-planned positions in ultrasound guided prostate implants. Radiol. Oncol. 1994; 32: 268–270.

[4] P. L. Roberson, V. Narayana, P. L. McShan, R. J. Winfield, and P. W. McLaughlin. Source placement error for permanent implant of the prostate, Med. Phys. 1997; 24: 251–257.

[5] R. Taschereau, J. Roy, and J. Pouliot. Monte Carlo simulations of prostate implants to improve dosimetry and compare planning methods. Med. Phys. Sept. 1999; 26 (9).

[6] J. Pouliot, R. Taschereau, C. Coté, J. Roy, and D. Tremblay. Dosimetric Aspects of Permanents Radioactive Implants for the Treatment of Prostate Cancer. Physics in Canada 1999; 55(2): 61-68.

[7] S. Cotin, H. Delingette, and N. Ayache. Real-Time Elastic Deformations of Soft Tissues for Surgery Simulation. IEEE Transactions on Visualization and Computer Graphics 1999; 5 (1).

[8] Y. Zhuang. Real-time Simulation of Physically Realistic Global Deformations. PhD. Thesis. 2000.

[9] X. Wu, M.S. Downes, T. Goktekin, and F. Tendick. Adaptive Nonlinear Finite Elements for Deformable Body Simulation Using Dynamic Progressive Meshes. In Proc. Eurographics 2001; 20 (3).

[10] G. Picinbono, H. Delingette, N. Ayache. Nonlinear and anisotropic elastic soft tissue models for medical simulation. IEEE Int. Conf. on Robotics and Automation 2001.

[11] S. P. DiMaio and S. E. Salcudean, Needle Insertion Modeling and Simulation. IEEE Int. Conf. on Robotics and Automation 2002.

[12] O.C. Zienkiewicz and R.L. Taylor. The Finite Element Method. 5th Ed. Butterworth-Heinemann. 2000.

[13] W. L. Wood. Some Transient and Coupled Problems – A State-of-the-Art Review. In: R. W. Lewis et. al., editors. Numerical Methods in Transient and Coupled Problems, Chapter 8. 1987.

[14] R. Alterovitz and K. Goldberg. Comparing Algorithms for Soft Tissue Deformation: Accuracy Metrics and Benchmarks. http://ford.ieor.berkeley.edu/ron/research/. 2002.

[15] C. Simone and A. M. Okamura. Modeling of Needle Insertion Forces for Robot-Assisted Percutaneous Therapy. IEEE Int. Conf. on Robotics and Automation 2002.

[16] D. Baraff and A. Witkin. Large Steps in Cloth Animation. Computer Graphics Proceedings, SIGGRAPH 1998: 43-54.